Three-Dimensional Quantitative Structure−Activity Relationships of ATP-Sensitive Potassium (K_{ATP}) Channel Openers Belonging to the 3-Alkylamino-4*H*-1,2,4-benzo- and 3-Alkylamino-4*H*-1,2,4-pyridothiadiazine 1,1-Dioxide Families

Pascal de Tullio,*[,†,‡] Léon Dupont,[§,‡] Pierre Francotte,[†] Stéphane Counerotte,[†] Philippe Lebrun,[⊥] and Bernard Pirotte[†]

Centre de recherche en Pharmacochimie des Substances Naturelles et Synthétiques, Laboratoire de Chimie Pharmaceutique, Université de Liège, 1 avenue de l'hôpital, B-4000 Liège, Belgium, Laboratoire de Pharmacodynamie et de Thérapeutique, Université Libre de Bruxelles, 808 route de Lennik, B-1070 Bruxelles, Belgium, and Unité de Cristallographie, Université de Liège, 17 Allée du 6 août, B-4000 Liège, Belgium

Received May 9, 2006

Recent studies have demonstrated that selective activation of pancreatic ATP-sensitive potassium (K_{ATP}) channels could be of clinical value in the treatment of type I and type II diabetes, obesity, and hypersinsulinemia. Taking into account these promising therapeutic opportunities, we have explored the 3-alkylamino-4*H*-1,2,4-pyrido- and 3-alkylamino-4*H*-1,2,4-benzothiadiazine 1,1-dioxide families. Among these series, numerous drugs were identified as highly potent and selective openers of either the pancreatic or the aortic K_{ATP} channels. Thanks to comparative molecular field analysis (CoMFA) and comparative molecular similarity indices analysis (CoMSIA), quantitative structure−activity relationship approaches using more than 100 compounds, pharmacophoric models explaining the activity and selectivity of the drugs have been elaborated. These models highlighted the importance of several chemical regions for K_{ATP} channel activation and could be very helpful for future improvement of drug potency, selectivity, or both. Moreover, an original CoMSIA analysis, using a selectivity index (SI) as a dependent variable, was also performed with the aim of identifying the structural parameters influencing tissue selectivity.

Introduction

Potassium channels regulated by changes in intracellular levels of adenosine triphosphate (K_{ATP} channels) have been identified in a wide range of cell types.[1−8] These channels are composed of two different protein subunits in a 4 + 4 stoichiometry[9] and link the metabolic state to the electrical activity of the cell. The K_{ATP} channel pore belongs to the inwardly rectifying potassium channel family[10] (Kir6.x.), while the second subunit (SURx for sulfonylurea receptor) contains the regulatory sites for most drugs.[10] Several subfamilies of variants of Kir6.x (Kir6.1 and Kir6.2) and several variants of SUR (SUR1, SUR2A, SUR2B) have been reported.[11] The combination of these different subunits can vary and lead to specific K_{ATP} channel subtypes. For example, SUR1 combines with Kir6.2 to form the insulin-secreting-cell K_{ATP} channel.[12] SUR2A and Kir6.2 subunits are found in cardiac and skeletal muscle, while the smooth muscle K_{ATP} channel is composed of SUR2B and Kir6.1 or Kir6.2 subunits.[13] Although pancreatic K_{ATP} channels are reported to be involved in the insulin-secreting process[14,15] and smooth muscle K_{ATP} channels in the control of muscle tone,[16,17] the physiological roles of the different channel subtypes have not yet been thoroughly assessed.[18]

Activation of K_{ATP} channels led to plasma membrane hyperpolarization. As a result, agents able to activate such channels (potassium channel openers or PCOs) have been shown to reduce the activity of different excitable cells.[19] Therefore, PCOs can interfere with several important physiological processes such as insulin release from pancreatic B-cells and contractile activity from smooth muscle cells.[21,22]

Selective activation of pancreatic K_{ATP} channels has been demonstrated to be of clinical value in the treatment of metabolic disorders such as type I and type II diabetes, obesity, and hyperinsulinemia.[23−26] A few years ago, diazoxide, an antihypertensive agent, was the only compound reported to activate pancreatic K_{ATP} channels. Unfortunately, as a consequence of its lack of tissue selectivity, diazoxide induced side effects, such as hypertrichosis, edema, headache, and arterial hypotension.[27] Thus, and in order to develop a new class of therapeutic agents, the pancreatic selectivity of the PCOs appears to be a key challenge. Taking into account the promising therapeutic value of pancreatic B-cell-selective PCOs, we have been interested, during the past decade, in the development of new compounds belonging to 3-alkylamino-4*H*-1,2,4-pyrido- and 3-alkylamino-4*H*-1,2,4-benzothiadiazine 1,1-dioxides. Such drugs can be considered as hybrid structures between **1** (diazoxide) and **2** (pinacidil) (Figure 1).[28−35] Several modulation poles were explored (Figure 1), including the nature of the subsituent on the exocyclic nitrogen atom in the 3-position, the position of the pyridinic nitrogen atom in the pyridothiadiazine heterocycle, the number, the nature, and the position of the subsituent(s) on the benzene ring of benzothiadiazine dioxides, and the presence of alkyl groups in the 2- and 4-positions. More than 200 drugs were synthesized and evaluated in vitro as potential PCOs. Among these drugs, **3** (BPDZ 44),[36] **4** (BPDZ 73),[37] **5** (BPDZ 154),[38] **6** (BPDZ 216),[39] and **7** (BPDZ 256)[35] (Figure 2) were identified as potent and selective pancreatic PCOs and might be considered as valuable substitutes for diazoxide in the treatment of glucose homeostasis disorders. More recently, the thienothiadiazine isosters **8** (NNC 55-0118) and **9** (NN-414)

* Corresponding author. Tel.: 32-(0)4-366-43-69. Fax: 32-(0)4-366-43-62. E-mail: P.deTullio@ulg.ac.be.

† Laboratoire de Chimie Pharmaceutique, Université de Liège.

‡ Contributed equally to the work.

§ Unité de Cristallographie, Université de Liège.

⊥ Laboratoire de Pharmacodynamie et de Thérapeutique, Université Libre de Bruxelles.

10.1021/jm060534w CCC: $33.50
Published on Web 10/26/2006

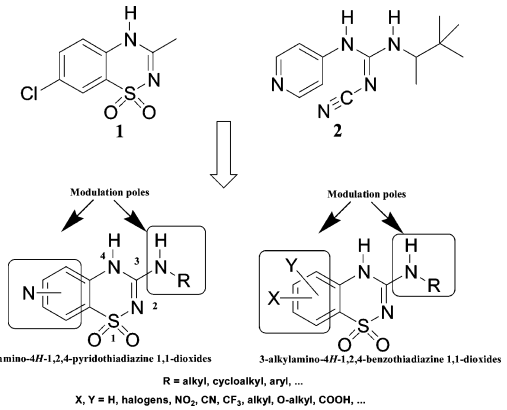

Figure 1. 3-Alkylamino-4*H*-1,2,4-pyrido- and 3-alkylamino-4*H*-1,2,4-benzothiadiazine 1,1-dioxides.

(Figure 2) have also been described and suggested for the treatment of metabolic disorders linked to insulin secretion.[40] Unfortunately, the development of NN-414 was stopped in phase II clinical trials because of an unwanted increase in blood liver enzymes, suggesting a liver toxicity.[41]

According to the potency and selectivity of several 3-alkylamino-4*H*-1,2,4-arylthiadiazine 1,1-dioxides on the SUR1/Kir6.2 K_{ATP} channel subtype, the determination of a pharmacophoric model appears to be crucial for the future chemical development of new SUR1/Kir6.2-selective compounds. Partial and fractional structure−activity relationships (SAR) previously deduced through a classical approach, from in vitro results, led to the first pharmacophoric model for activity on the pancreatic tissue (Figure 3).[28]

To confirm and to improve this initial model, but also to develop a pharmacophoric model for the activity on the vascular smooth muscle tissue, we decided to apply the comparative molecular field analysis (CoMFA)[a] and comparative molecular similarity indices analysis (CoMSIA) approaches to a series of 150 drugs belonging to the 3-alkylamino-4*H*-1,2,4-pyrido- and 3-alkylamino-4*H*-1,2,4-benzothiadiazine 1,1-dioxide series. A particular and original CoMSIA analysis, using a selectivity index (SI) as dependent variable, was also performed with the aim of identifying the structural parameters that influence tissue selectivity.

Computational Details

Data and Biological Activity. The training and the test sets for the 3D-QSAR studies were taken from a data set consisting of 136 compounds designed and synthesized at the Department of Medicinal Chemistry of the University of Liège according to procedures described in the literature.[28−35] The drugs were tested on two different pharmacological models: a pancreatic model onto which the ability of the compounds to inhibit glucose-induced insulin secretion was evaluated on isolated rat pancreatic islets (a model that could reflect the activation of the SUR1/Kir6.2 K_{ATP} channel subtype) and a vascular model onto which the ability of the compounds to reduce the contractile activity of KCl-depolarized rat aorta rings was measured (a model expected to reflect the activity of the drugs on the SUR2B/Kir6.1 channel subtype). The biological data obtained as IC_{50} (drug concentration, in micromolar, inhibiting 50% of the 16.7 mM glucose-induced insulin release) and EC_{50} (drug concentration, in micromolar, giving 50% relaxation of the 30 mM KCl-induced contraction) were converted into pIC_{50} (−log IC_{50}, Table 1) and pEC_{50} (−log EC_{50}, Table 1) values and used as dependent variables in the 3D-QSAR analyses. A selectivity index (SI), which represents the ratio between the EC_{50} and IC_{50} values was also calculated, converted into pSI (log SI, Table 1), and used as a dependent variable in a particular CoMSIA analysis. The structure of the compounds and the biological data are listed in Table 1.

Molecular Modeling and Alignment. Molecular modeling studies of the compounds were performed using the SYBYL 7.0[42] software package, Tripos Associates (St. Louis, MO), on a Silicon Graphics O2 workstation. Molecular structures were built using the built/edit commands of SYBYL starting from 27 crystal structures previously determined. All values were filled with valence, and MOPAC[43] (method AM1) charges were calculated for each compound. Geometry optimization was carried out using MAXIMIN2 molecular mechanics and Tripos force field supplied within SYBYL, with convergence criterion set at 0.05 kcal/(Å mol). Systematic conformational search was also carried out to recognize a reasonably low-energy conformation for each compound. For drugs exhibiting a stereogenic center on the 3-alkylamino side chain, only the racemates were introduced in the study and built as the *R*-enantiomeric structure. This necessary arbitrary choice was driven by classical SAR deduced from the comparison of biological data obtained with (*R*)- and (*S*)-BPDZ 42 and -BPDZ 44 enantiomers.[44] The orientation of the 3-alkylamino side chain deduced from these molecules after molecular modeling fixed the orientation of the chains for all the other compounds.

A superimposition of molecules was first realized by trying to minimize root-mean-square (rms) differences in the fitting of selected atoms (the 10 atoms of the fused rings) with those of a template molecule (**5**). The field fit procedure was then used as the second alignment criteria to increase field similarity within the entire molecular data set. In the field fit operation, the rms difference in the sum of steric and electrostatic interaction energies averaged across all lattice points between molecules in the training set and the template molecule was minimized to find the best fit. The steric and electrostatic fields were evaluated from the QSAR CoMFA FIELD process.

CoMFA and CoMSIA 3D QSAR Analysis. CoMFA and CoMSIA models were generated using SYBYL 7.0. The CoMFA steric and electrostatic fields and the CoMSIA molecular descriptor fields, expressed as steric, electrostatic, hydrophobic, hydrogen bond donors, and hydrogen bond acceptors, were calculated using the default settings in SYBYL and correlated with the variations of the target properties [pIC_{50} (−log IC_{50}), pEC_{50} (−log EC_{50}), or pSI (log EC_{50}/IC_{50})] using the statistical method of partial least squares (PLS).[43] The "leave-one-out" (LOO) cross-validated method was applied to determine the optimum number of PLS components, corresponding to the highest r^2 (q^2) value and to the lowest standard error of prediction, *s*. The optimum of six components was used in the validation of the CoMFA model, and seven components were used in the validation of the CoMSIA analysis. The un-cross-validated models were assessed by the explained variance r^2, standard error of estimated *S*, and *F* ratio. The CoMFA analysis was only undertaken on the pIC_{50} values to test the homogeneity of the whole data set and to evaluate the fields used in the field fit procedure. Statistical results obtained from field fit alignment criteria gave better cross-validated q^2 values than superimposition (data not shown) in the earliest studied models. Therefore, only field fit alignment was used for further CoMFA and CoMSIA studies. In the final CoMFA analysis, 126 compounds were used, omitting the most outlying compounds **135** (BPDZ 61), **122** (BPDZ 80), **123** (BPDZ 81), **44** (BPDZ 274), and **45** (BPDZ 275). The pIC_{50} CoMSIA analysis included 130 compounds (the most outlying **135** was omitted), and the pEC_{50} CoMSIA analysis was based on 107 compounds (omitting **67** (BPDZ 70), **70** (BPDZ 158), **93** (BPDZ 190), **24** (BPDZ 214), and **84** (BPDZ 243)). The pSI CoMSIA comprised 106 derivatives, the most outlying **12** (BPDZ 137) being excluded in addition to those omitted in the previous pIC_{50} and pEC_{50} CoMSIA analysis. Except for **44** (BPDZ 274) and **45** (BPDZ 275), which have the singular 7-cyano substituent included in the

[a] Abbreviations: QSAR, quantitative structure−activity relationship; CoMFA, comparative molecular field analysis; CoMSIA, comparative molecular similarity indices analysis; PLS, partial least squares; pIC_{50}, −log IC_{50}; pEC_{50}, −log EC_{50}; pSI, log EC_{50}/IC_{50}.

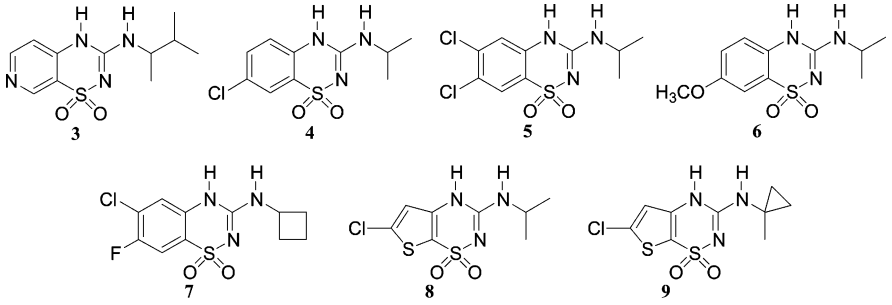

Figure 2. Chemical structures of the most interesting drugs.

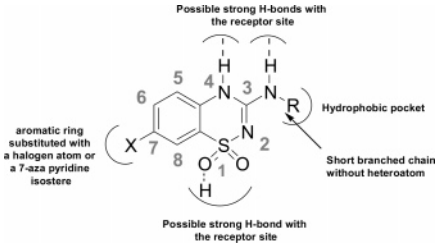

Figure 3. Initial pharmacophoric model for the activity on the pancreatic endocrine tissue.

analysis, we were unable to find any structural explanation for the removal of the other compounds.

QSAR Coefficient Contour Maps. The visualization of the results of the best CoMSIA models have been performed using "Coeff × SD" mapping option contoured by actual values. The maps were generated by interpolation of the pairwise products between the PLS coefficients (Coeff) and the standard deviations (SD) of the corresponding CoMSIA descriptor values. The contours of the CoMSIA steric map are shown in green (more bulk favorable) and yellow (less bulk favorable). The electrostatic fields contours are colored blue (positive charge favorable) and red (negative charge favorable). The contours of the hydrophobic fields are colored yellow (hydrophobic groups enhance activity) and white (hydrophilic groups enhance activity). The hydrogen bond acceptor field contours show regions where hydrogen bond acceptors (magenta) on the drugs are favorable for activity or regions where hydrogen bond donors on the receptor site enhance the activity. The regions where hydrogen bond acceptors on the receptor site enhance the activity are colored red. As the positive log EC_{50}/IC_{50} target values were used in the EC/IC CoMSIA analysis, the maps need to be interpreted as a function of the pSI quotient. Therefore, a green region in a steric map is more discriminating for the IC_{50}, whereas a yellow region is more discriminating for the EC_{50}. In each CoMSIA analysis, the contribution of the hydrogen bond donor field description is very low, and no contour map of this property is shown.

Results and Discussion

The Pancreatic Model. **Results of the CoMFA Analysis.** The statistical data obtained from the standard CoMFA model constructed with steric and electrostatic fields are shown in Table 2. The main objective of CoMFA analysis was to optimize the different parameters in order to find the best predictive model. Superimposition and field fit were the two alignment criteria used in our CoMFA study. Statistical results obtained from field fit alignment criteria gave better cross-validated r^2 (q^2) values than superimposition (data not shown) for the IC_{50} analysis. Therefore, only field fit alignment was used for further QSAR 3D (CoMSIA) studies. The default setting column filtering 2.0 kcal/mol was used to evaluate the optimal number of components (6) using the leave-one-out (LOO) cross-validated analysis. A q^2 value of 0.682 was obtained, indicating a good predictive capacity of the model ($q^2 > 0.5$). A satisfactory correlation coefficient (r^2) of 0.842 for the un-cross-validated indicates self-consistency of the model. The steric and electrostatic fields contributed to the QSAR equation by 72.0% and 28.0%, respectively.

Results of the CoMSIA Analysis. The statistical data obtained from the standard CoMSIA model constructed with steric, electrostatic, hydrophobic, and H-bond donor and acceptor fields are also reported in Table 2. The default setting column filtering 2.0 kcal/mol was used to evaluate the optimal number of components (7) using the leave-one-out (LOO) cross-validated analysis. As noted for the CoMFA analysis, the q^2 (0.693) and the r^2 values (0.842) are consistent with a good predictive capacity and self-consistency of the model. The hydrophobic field markedly contributed to the QSAR equation (by 42.7%), while contribution of the H-bond acceptor field was about 23.0%, and the steric and electrostatic fields contributed 14.9% and 17.1%, respectively (the percentage of the H-bond donor field is insignificant). Surprisingly, the important steric contribution observed in the CoMFA analysis was not found in the CoMSIA corresponding model. The predicted versus actual pIC_{50} and the residual (pIC_{50} act. − pIC_{50} pred.) values of the training set are presented in the Supporting Information. It should be noticed that the residual values almost increased uniformly from 0.0002 to 0.917, independently of the nature of the substituent R, X, or Y on the molecule.

Besides internal validation with the training set, an external test set of five compounds (**141**−**145**, Figure 1) was used to validate the predictivity of the model. The corresponding predicted, actual, and residual values are given in the Supporting Information. Prior to prediction, the test set compounds were processed identically to the training set compounds as described in the Computational Details section. The predicted affinities for the test set are all in a reasonable agreement with the experimental values. No outlier values were observed among the five test set molecules.

CoMSIA Contour Map Analysis. In Figure 4, the electrostatic, steric, hydrophobic, and hydrogen bond acceptor fields are shown as contour maps for the pancreatic model.

Concerning the electrostatic field properties (Figure 4A), the large red contour region centered on the substituent group at the 7-position indicates that the presence of negative charges (due to electronegative atoms such as chlorine, fluorine, or oxygen) could be favorable for activity. A significant blue region appearing on the alkyl part of the 3-alkylamino side chain suggests that positive charges could increase activity (or negative charges decrease activity). This feature could be due to the deleterious impact of an electroattracting group (i.e., CF_3). The presence of a blue region located near the 8-position is less easily explainable, even if the presence of a nitrogen atom at this position (pyridinic series) leads to a drastic decrease of activity.

Examination of the steric field map clearly demonstrates the influence of the steric environment on activity (Figure 4B). A

Table 1. Structure and Pharmacological Data of the Training and of the Test Sets Used in the 3D-QSAR Analysis

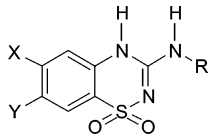

Benzenic Series Training Set

no.	X	Y	R	pIC_{50}[e]	pEC_{50}[f]	pSI[g]	no.	X	Y	R	pIC_{50}[e]	pEC_{50}[f]	pSI[g]
10	H	Br	$CH(CH_3)_2$	0.268	−0.681	0.949	**66**	H	I	$CH(CH_3)_2$	−0.143	−1.114	0.971
11	H	Br	$CH(CH_3)C_2H_5$	−0.772	−0.748	−0.023	**67**	H	I	$CH(CH_3)C_2H_5$	−1.290	−1.580	0.290
12	H	Br	$CH(CH_3)CH(CH_3)_2$	−1.520	−0.415	−1.105	**68**	H	I	$CH(CH_3)CH(CH_3)_2$	−1.712	0.046	−1.758
13	H	Br	$CH(CH_2)_2$[a]	−0.616	−1.951	1.335	**69**	H	I	$CH(CH_3)CH(CH_3)_3$	−1.360	−0.875	−0.485
14	H	Br	CH_3	−0.193	−1.490	1.298	**70**	H	I	$CH(C_2H_5)_2$	−1.160	−1.898	0.738
15	H	Br	C_2H_5	0.208	−0.792	1.000	**71**	H	I	$CH(CH_2)_3$[b]	−0.640	−1.346	0.707
16	H	Br	$CH(CH_2)_3$[b]	−0.065	−1.336	1.272	**72**	H	NO_2	$CH(CH_3)_2$	−1.125	−1.364	0.239
17	H	Br	CH_2CF_3	−1.480			**73**	H	NO_2	$CH(CH_3)C_2H_5$	−1.950	−0.785	−1.165
18	H	Br	$CH_2CH_2CH_3$	−0.778	−0.771	−0.007	**74**	H	NO_2	$CH(CH_3)CH(CH_3)_2$	−2.355	−0.447	−1.908
19	H	Br	$CH_2CH{=}CH_2$	−0.530	−0.477	−0.052	**75**	H	NO_2	$CH_2CH(CH_2)_2$[a]	−2.430		
20	H	CF_3	$CH(CH_3)_2$	−0.279	−1.117	0.839	**76**	H	NO_2	$CH_2CH_2CH_3$	−2.330	−1.196	−1.134
21	H	CF_3	$CH(CH_3)C_2H_5$	−1.440	−0.949	−0.491	**77**	H	NO_2	$CH(CH_2)_3$[b]	−1.900	−1.140	−0.760
22	H	CF_3	$CH_2CH_2CH_3$	−1.790	−0.462	−1.328	**78**	H	OC_2H_5	C_2H_5	−1.390	−2.211	0.821
23	H	CF_3	$CH_2CH(CH_2)_2$[a]	−2.170	−1.004	−1.166	**79**	H	OC_2H_5	$CH(CH_3)_2$	−1.237	−2.368	1.131
24	H	CH_3	$CH(CH_3)_2$	−0.298	−2.301	2.004	**80**	H	OC_2H_5	$CH(CH_2)_3$[b]	−1.560	−2.602	1.042
25	H	CH_3	$CH(CH_2)_3$[b]	−0.745	−1.766	1.021	**81**	H	OCH_3	$CH(CH_3)_2$	−0.255	−2.438	2.182
26	H	Cl	$CH(CH_3)CH(CH_3)_2$	−0.750	−0.303	−0.447	**82**	H	OCH_3	$CH_2CH_2CH_3$	−0.990	−2.602	1.612
27	H	Cl	$CH(CH_3)_2$	0.113	−1.502	1.616	**83**	H	OCH_3	$CH(CH_3)C_2H_5$	−0.655	−1.243	0.588
28	H	Cl	$CH(CH_3)C_2H_5$	−0.570	−1.582	1.013	**84**	H	OCH_3	$CH(CH_2)_3$[b]	−0.380	−0.079	−0.301
29	H	Cl	$CH(CH_3)CH(CH_3)_3$	−0.960	−1.109	0.149	**85**	H	OCH_3	$CH(CH_3)CH_2OH$	−0.830		
30	H	Cl	$CH(CH_2)_2$[a]	−0.645	−2.279	1.634	**86**	F	F	C_2H_5	0.000	−1.824	1.824
31	H	Cl	$CH(CH_2)_3$[b]	−0.043	−1.543	1.501	**87**	F	H	$CH(CH_2)_3$[b]	−0.124	−2.602	2.478
32	H	Cl	CH_2CF_3	−1.240			**88**	F	H	$CH(CH_3)_2$	−0.053	−2.290	2.237
33	H	Cl	CH_3	−0.072	−2.151	2.079	**89**	Cl	Br	$CH(CH_3)_2$	0.579	−0.748	1.333
34	H	Cl	CH_2CH_3	0.284	−1.600	1.884	**90**	Cl	Br	$CH(CH_2)_3$[b]	−0.110	−0.822	0.712
35	H	Cl	$CH_2CH_2CH_3$	−0.431	−1.744	1.313	**91**	Cl	Br	C_2H_5	0.553	−0.515	1.067
36	H	Cl	$CH_2CH{=}CH_2$	−0.558	−1.461	0.903	**92**	Cl	Cl	$CH(CH_3)_2$	0.553	−0.358	0.911
37	H	Cl	$CH_2CH(CH_2)_2$[a]	−1.219	−1.615	0.396	**93**	Cl	Cl	$(CH_2)_5CH_3$	−1.640	−2.367	0.727
38	H	Cl	$CH(CH_3)CH_2OCH_3$	−1.750			**94**	Cl	Cl	$CH(CH_2)_2$[a]	−0.650		
39	H	Cl	$CH(C_2H_5)_2$	−0.799	−1.971	1.172	**95**	Cl	Cl	$CH(CH_2)_3$[b]	−0.083	−0.555	0.472
40	H	Cl	$CH_2CH(CH_3)OH$	−1.890	−2.602	0.712	**96**	Cl	Cl	C_2H_5	0.664	−0.081	0.557
41	H	Cl	$CH(CH_3)CH_2OH$	−0.588	−1.732	1.145	**97**	Cl	Cl	$CH_2CH{=}CH_2$	−0.287	−0.079	−0.206
42	H	Cl	$(CH_2)_5CH_3$	−1.520	−0.708	−0.811	**98**	Cl	Cl	$CH(CH_3)CH_2OH$	−0.134	−1.246	1.112
43	H	Cl	$CH(CH_3)CH_2OCOCH_3$	−0.580			**99**	Cl	Cl	$CH_2CH_2CH_3$	−0.079	−0.676	0.597
44	H	CN	$CH(CH_3)_2$	−1.370	−1.630	0.260	**100**	Cl	F	C_2H_5	0.824	−1.627	2.451
45	H	CN	$CH(CH_2)_3$[b]	−1.820	−1.763	−0.058	**101**	Cl	F	$CH(CH_2)_3$[b]	0.682	−1.601	2.279
46	H	F	$CH(CH_3)_2$	0.042	−1.635	1.681	**102**	Cl	F	$CH(CH_3)C_2H_5$	0.319	−1.326	1.645
47	H	F	$CH(CH_3)C_2H_5$	−0.139	−1.593	1.453	**103**	Cl	F	$CH_2CH_2CH_3$	0.215	−1.656	1.871
48	H	F	$CH(CH_3)CH(CH_3)_2$	−0.445	−1.422	0.976	**104**	Cl	F	$CH(CH_3)_2$	0.932	−1.618	2.539
49	H	F	C_2H_5	0.167	−2.602	2.770	**105**	Cl	H	C_2H_5	0.299	−1.739	2.040
50	H	F	$CH_2CH_2CH_3$	−0.280	−2.220	1.941	**106**	Cl	H	$CH(CH_2)_2$[a]	−0.590	−2.193	1.603
51	H	F	$CH(CH_2)_2$[a]	−0.820	−2.602	1.783	**107**	Cl	H	$CH(CH_2)_3$[b]	−0.190	−2.602	2.412
52	H	F	$CH(CH_2)_3$[b]	−0.077	−2.053	1.978	**108**	Cl	H	CH_2CF_3	−0.766		
53	H	F	$CH(CH_2)_4$[c]	−0.126	−1.763	1.639	**109**	Cl	H	$CH_2CH_2CH_3$	−0.322	−1.864	1.542
54	H	F	$CH_2CH(CH_2)_2$[a]	−0.946	−2.164	1.218	**110**	Cl	H	$CH_2CH(CH_2)_2$[a]	−0.960		
55	H	F	$CH_2CH{=}CH_2$	−0.470	−2.602	2.132	**111**	Cl	H	$CH_2CH{=}CH_2$	−0.330	−2.167	1.837
56	H	F	$CH(CH_3)CH_2OCH_3$	−1.520			**112**	Cl	H	$CH(CH_2)_4$[c]	−0.440	−2.602	2.163
57	H	F	CH_3	−0.342	−2.602	2.260	**113**	Cl	H	$CH(CH_2)_5$[d]	−1.187		
58	H	F	CH_2CF_3	−1.490			**114**	Cl	H	$CH(CH_3)CH_2OH$	−0.188	−2.302	2.115
59	H	F	$CH(CH_3)CH_2OH$	−0.582	−2.602	2.020	**115**	Cl	OCH_3	C_2H_5	0.208	−0.908	1.116
60	H	H	$CH(CH_3)_2$	−0.610	−2.602	1.992	**116**	Cl	OCH_3	$CH(CH_3)_2$	0.602	−1.568	2.170
61	H	H	C_2H_5	−1.056	−2.602	1.546	**117**	Cl	OCH_3	$CH(CH_2)_3$[b]	0.208	−1.369	1.577
62	H	H	$CH(CH_3)C_2H_5$	−0.850			**118**	Br	H	C_2H_5	0.475	−1.723	2.205
63	H	H	$CH(CH_2)_3$[b]	−0.630			**119**	Br	H	$CH(CH_3)_2$	0.658	−1.746	2.403
64	H	H	$CH(CH_2)_4$[c]	−0.754			**120**	Br	H	$CH(CH_2)_3$[b]	0.187	−2.602	2.789
65	H	H	$CH_2CH_2CH_3$	−1.040			**121**	Br	H	$CH(CH_3)CH_2OH$	−0.295		

wide and unique favorable region (green) is found on a side of the alkyl chain at the 3-position, while a smaller unfavorable steric field (yellow) appears farther on this chain. Such data underline the importance of the substitution at the 3-position by a short but also branched alkyl chain. A broad unfavorable region (yellow) is also present near the 7-position and indicates that bulky groups (such as Br, I, OC_2H_5) have a negative impact on activity. No negative or positive information could be deduced concerning the 6-position, suggesting that the nature of the substituent at this position is less critical for activity.

The contribution map of hydrophobic fields is described in Figure 4C. The presence of a hydrophobic propitious region (yellow) at the 7-position confirms the positive impact of a halogen atom on activity, while the small hydrophilic favorable regions (white) are probably due to OCH_3 substitution but also

Table 1. Continued

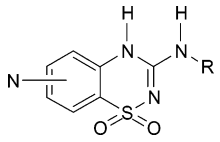

Pyridinic Series Training Set

no.	N position	R	pIC_{50}[e]	pEC_{50}[f]	pSI[g]	no.	N position	R	pIC_{50}[e]	pEC_{50}[f]	pSI[g]
122	5-aza-7-chloro	$CH(CH_3)_2$	−2.120	−1.164	−0.956	**132**	7-aza	$CH(CH_3)CH(CH_3)_2$	−0.646	−2.097	1.451
123	5-aza-7-chloro	$CH(CH_3)C_2H_5$	−1.940	−1.300	−0.640	**133**	7-aza	$CH(CH_2)_4$[c]	−1.440	−2.778	1.338
124	5-aza-7-chloro	$CH(CH_3)CH(CH_3)_2$	−1.896	−1.083	−0.813	**134**	7-aza	$CH(CH_2)_5$[d]	−1.716	−2.699	0.983
125	5-aza-7-chloro	$CH(CH_3)C(CH_3)_3$	−1.630	−0.017	−1.613	**135**	7-aza	C_2H_5	−1.895	−2.778	0.883
126	5-aza-7-chloro	$(CH_2)_5CH_3$	−1.640			**136**	7-aza	$CH(CH_3)C(CH_3)_3$	−0.580	−1.165	0.585
127	7-aza	$CH_2CH_2CH_3$	−1.750	−2.778	1.028	**137**	7-aza	$CH(C_2H_5)_2$	−0.852	−1.609	0.757
128	7-aza	$CH(CH_3)_2$	−1.008	−2.602	1.594	**138**	7-aza	$(CH_2)_5CH_3$	−1.870	−2.025	0.155
129	7-aza	$(CH_2)_3CH_3$	−1.620	−2.778	1.158	**139**	8-aza	$CH(CH_3)_2$	−1.480		
130	7-aza	$CH(CH_3)C_2H_5$	−0.623	−2.312	1.689	**140**	8-aza	$CH(CH_3)CH(CH_3)_2$	−1.250		
131	7-aza	$CH_2CH(CH_3)_2$	−1.315	−2.313	0.999						

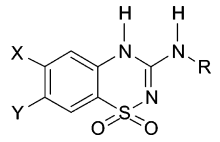

Test Set

no.	X	Y	R	pIC_{50}[e]	pEC_{50}[f]	pSI[g]	no.	X	Y	R	pIC_{50}[a]	pEC_{50}[b]	pSI[c]
141	H	CH_3	$CH(CH_3)_2$	−0.301	−2.301	2.000	**144**	H	CH_3	CH_2CH_3	−0.398	−2.323	1.925
142	F	F	$CH(CH_3)_2$	0.523	−2.009	2.531	**145**	H	CH_3	$CH(CH_3)CHCH_2CH_3$	−1.049	−1.190	0.141
143	F	F	$CH_2CH(CH_3)_2$	−0.754	−2.301	1.547							

[a] Cyclopropyl. [b] Cyclobutyl. [c] Cyclopentyl. [d] Cyclohexyl. [e] −log IC_{50}. [f] −log EC_{50}. [g] log(EC_{50}/IC_{50}).

Table 2. Summary of CoMFA and CoMSIA Results for Various Models[a]

	CoMFA	CoMSIA		
	pancreatic model	pancreatic model	aortic model	selectivity model
	Leave-One-Out (LOO) Cross-Validated			
q^2	0.682	0.693	0.673	0.763
s	0.440	0.442	0.448	0.542
F	42.871	39.753	29.043	43.097
n	126	130	107	106
n_1	6	7	7	7
n_2	120	123	99	97
vars	1170	1170	1170	1170
	Un-Cross-Validated			
r^2	0.842	0.842	0.795	0.861
S	0.310	0.318	0.354	0.415
F	106.772	93.404	55.015	85.845
n	127	131	107	105
n_1	6	7	7	7
n_2	120	123	99	97
vars	1170	1170	1170	1170
	Contributions			
steric	0.724	0.149	0.096	0.146
electrostatic	0.276	0.171	0.086	0.092
hydrophobic		0.427	0.603	0.539
H-bond donor		0.023	0.006	0.008
H-bond acceptor		0.230	0.209	0.216

[a] q^2, the leave-one-out (LOO) cross-validated coefficient, $q^2 = 1{,}0 - [\mathrm{PRESS}/\sum_{(Y)}(Y_{\mathrm{actual}} - Y_{\mathrm{mean}})^2]$; PRESS (predictive error sum of squares) $= \sum_{(Y)}(Y_{\mathrm{pred}} - Y_{\mathrm{actual}})^2$; Y_{pred} is a predicted value; Y_{actual} is an actual or experimental value; Y_{mean} is the best estimate of the mean of all values that might be predicted; $s = \sqrt{(\mathrm{PRESS}/n_2)}$, the standard error of prediction in the LOO cross-validated analysis; S, the standard error of estimate in the un-cross-validated analysis; r^2, the squared conventional correlation coefficient; F, F-statistic $= r^2/(1.0 - r^2)$; n, number of compounds; n_1, the number of components giving the lowest PRESS value (optimal number of components); $n_2 = n - n_1 - 1$; vars, number of explanatory variables by property.

to the negative influence of too bulky subtituents. The white region on the alkyl side chain at the 3-position probably results from the presence of a hydroxy group.

The hydrogen bond acceptor map clearly delineates, near the 6-position and near the 3-alkylamino side chain, several regions where hydrogen bond acceptors (magenta) enhance the activity

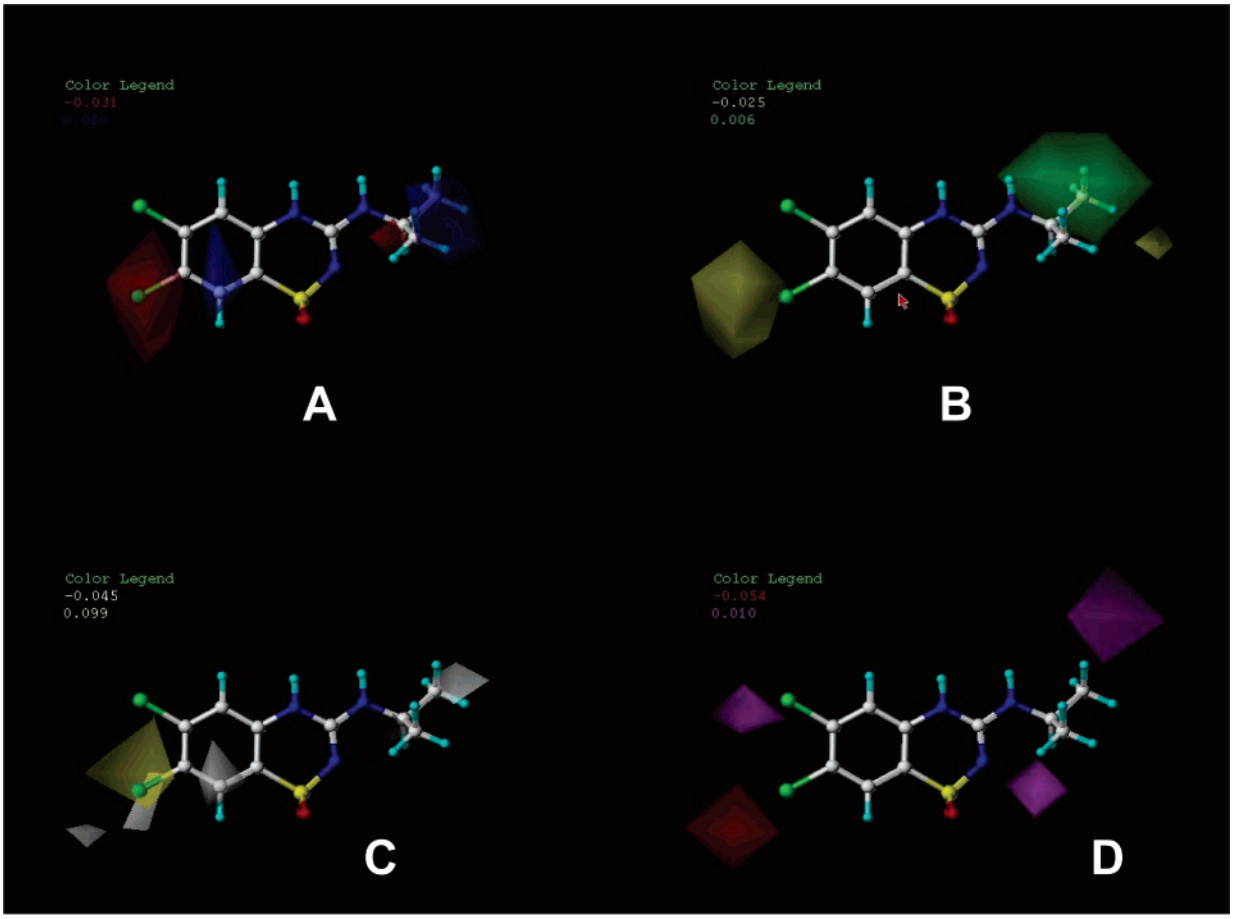

Figure 4. CoMSIA contour maps for the pancreatic model: (A) electrostatic properties, the blue isocontours denote regions where positively charged groups could increase activity (contour level 0.020) and red areas indicate enhanced activity with negatively charged groups (contour level −0.031); (B) steric properties, sterically favorable areas are shown in green (contour level 0.006), while the yellow isocontours depict sterically deleterious areas (contour level −0.025); (C) hydrophobic properties, yellow polyhedra (contour level 0.099) indicate regions where hydrophobic groups could enhance activity and white areas (contour level −0.045) depict regions where hydrophilic groups could favor activity; (D) H-bond acceptor properties, magenta isocontours (contour level 0.010) depict areas where H-bond acceptors on the molecule (or H-bond donors on the receptor site) could favor activity; the corresponding unfavorable areas are shown in red (contour level −0.054).

(Figure 4D). These data are in accordance with a classical SAR analysis. In contrast, near the 7-position, a negative effect of acceptors (red) is predicted and probably reflects the drastic decrease of activity noticed with the 7-NO_2, 7-CN, and 7-CF_3 derivatives.

The Aortic Model. Results of the CoMSIA Analysis. The statistical data obtained from the CoMSIA analysis for the aortic model are shown in Table 2. The process and the results are similar to those of the pancreatic model. The q^2 (0.673) and the r^2 (0.795) values are, nevertheless, slightly lower. Thus, the aortic model can be considered of lower quality. The importance of the hydrophobic properties seems to be higher with a contribution of the hydrophobic field of about 60.3%. On the other hand, the contribution of the steric and electrostatic fields are lower (9.6% and 8.6% respectively). The predicted versus actual pEC_{50} and the residual (pEC_{50} act. − pEC_{50} pred.) values of the training set are reported in the Supporting Information. As in the pancreatic model, the residual values almost increased uniformly from 0.003 to 1.030, independently of the substituents R, X, or Y on the molecule.

An external test set of five compounds (**141**−**145**, Figure 1) was also used to validate the predictivity of the model. The corresponding predicted, actual, and residual values are given in the Supporting Information. As in the pancreatic model, the predicted affinities for the same test set are all in a reasonable agreement with the experimental values.

CoMSIA Contour Map Analysis. The contour maps for the electrostatic, steric, hydrophobic, and hydrogen bond acceptor fields are presented in Figure 5.

Figure 5A illustrates the electrostatic properties. Two favorable negative red contour regions are found around the substituent group at the 7-position (not centered on this group). These regions probably indicate that bulky electronegative groups could have a positive impact on the myorelaxant activity of the drugs (i.e., bromine and iodine atoms, NO_2 and CF_3 groups). As noticed for the pancreatic model, an important positive blue region also appears on the alkyl part of the 3-alkylamino side chain and could be due to the deleterious impact of an electron-attracting group (i.e., CF_3). The presence of a blue region around the aryl nucleus proves that an aromatic ring with a low electronic density can be favorable for the vasorelaxant activity.

Examination of the steric field map (Figure 5B) led to the conclusion that the presence of a bulky substituent at the 7-position (green) is not deleterious for activity (except for very long substituents such as a pentyl group). Two favorable regions (green) are also found on a side of the alkyl chain at the 3-position, while a marked unfavorable steric field (yellow) appears farther on this chain. These data underline the importance of the substitution at the 3-position by a branched alkyl chain and the deleterious effect of a small ring (cyclopropyl, cyclobutyl) on the myorelaxant activity of the compounds. No

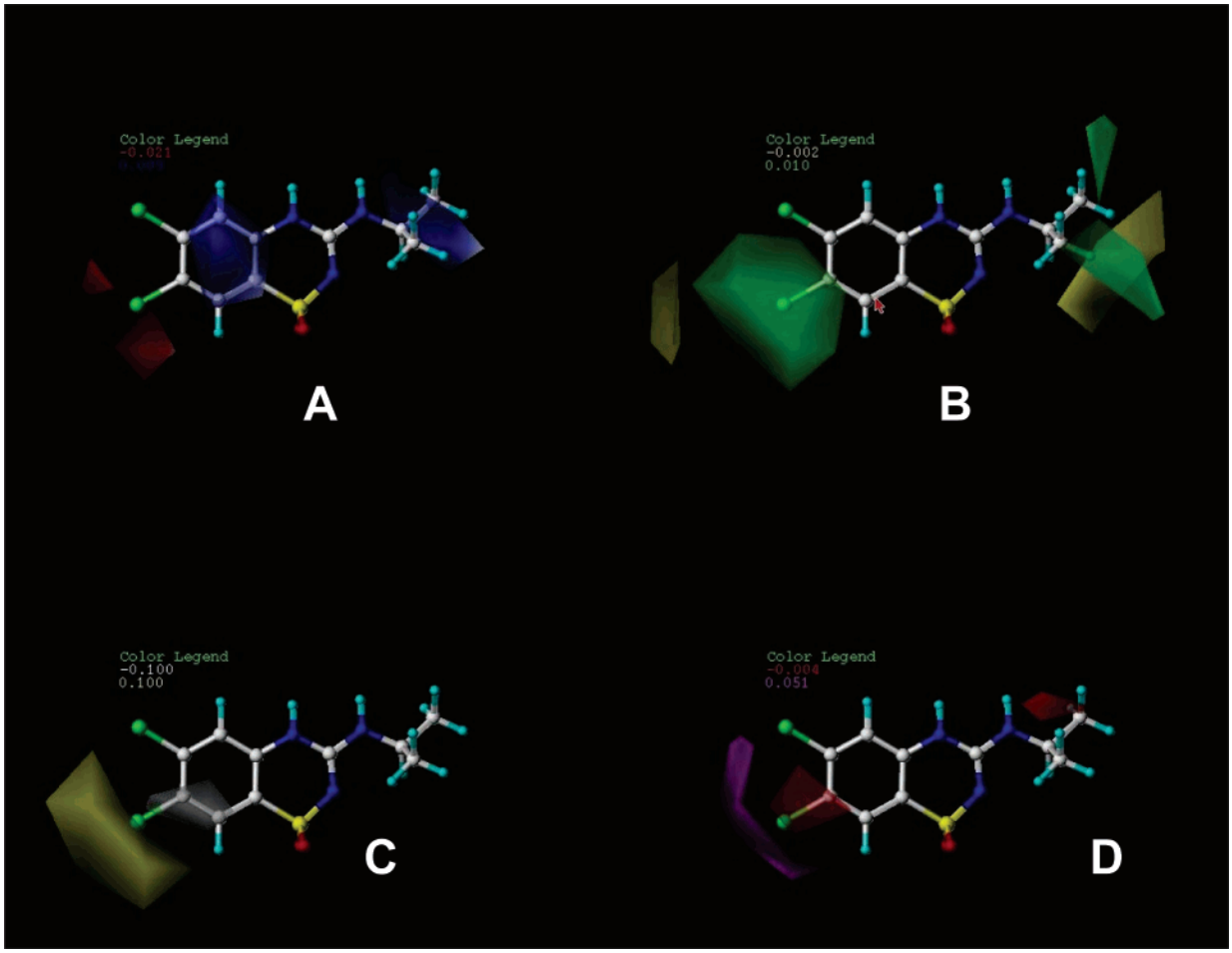

Figure 5. CoMSIA contour maps for the aortic model: (A) electrostatic properties, the blue isocontours denote regions where positively charged groups could increase activity (contour level 0.009) and red areas indicate enhanced activity with negatively charged groups (contour level −0.021); (B) steric properties, sterically favorable areas are shown in green (contour level 0.010), while the yellow isocontours depict sterically deleterious areas (contour level −0.002); (C) hydrophobic properties, yellow polyhedra (contour level 0.100) indicate regions where hydrophobic groups could enhance activity and white areas (contour level −0.100) depict regions where hydrophilic groups could favor activity; (D) H-bond acceptor properties, magenta isocontours (contour level 0.051) depict areas where H-bond acceptors on the molecule (or H-bond donors on the receptors site) could favor activity; the corresponding unfavorable areas are shown in red (contour level −0.004).

negative or positive impacts are detected for the 6-position, reinforcing the view that the substitution at this position does not appear to be critical for activity.

In this pharmacological model, hydrophobic fields are the most important contributors for the CoMSIA analysis. The presence of a wide hydrophobic region (yellow) near the 7-position confirms the positive impact of a bulky group on activity (Figure 5C). No information was available for the side chain at the 3-position.

The role of the hydrogen bond acceptor properties seems to be trivial although the map indicates that hydrogen bond acceptors (magenta) only enhance the activity when located near the 7-position (Figure 5D). The presence of red regions centered on the 7-position or near the 3-alkylamino side chain is less easily explainable.

All these data, taken together with the classical SAR analyses, lead us to propose the first pharmacophoric model for vasorelaxant activity in the 3-alkylamino-4*H*-1,2,4-benzo- and 3-alkylamino-4*H*-1,2,4-pyridothiadiazine 1,1-dioxide series.

The Selectivity Model. Results of the CoMSIA Analysis. Table 2 also illustrates the statistical results of the CoMSIA analysis for the selectivity model where $\log(EC_{50}/IC_{50})$ was chosen as the dependent value. The q^2 (0.763) and r^2 (0.861) values are higher than in each individual model. However, the results of this analysis are not more accurate than those obtained with the previous pancreatic and aortic CoMSIA models. The contributions of the hydrophobic (53.9%) and H-acceptor fields (21.6%) are actually intermediate. The steric contribution (14.6%) is close to that found in the pancreatic model, and the electrostatic contribution (9.2%) is similar to that exhibited by the aortic model. The predicted versus actual pSI and the residual (pSI act. − pSI pred.) values are presented in the Supporting Information. As was predictable from the results on the pancreatic and on the previously reported aortic models, the residual values almost increased uniformly from 0.009 to 0.811, independently of the substituents R, X, or Y on the molecule.

CoMSIA Contour Map Analysis. The analysis of the contour maps is more delicate and should be used cautiously to predict which structural zones are important for the improvement of tissue selectivity (pancreatic versus aortic tissue). This original approach, coupled with the more classical CoMSIA analysis using the pharmacological data as dependent variables, could also be helpful for the rational design of more potent and tissue selective K_{ATP} channel openers.

Figure 6 depicts the electrostatic, steric, hydrophobic, and hydrogen bond acceptor contour maps. The analysis of these maps can be conducted in terms of favorable zones for activity on the pancreatic tissue or favorable zones for activity on the aortic tissue.

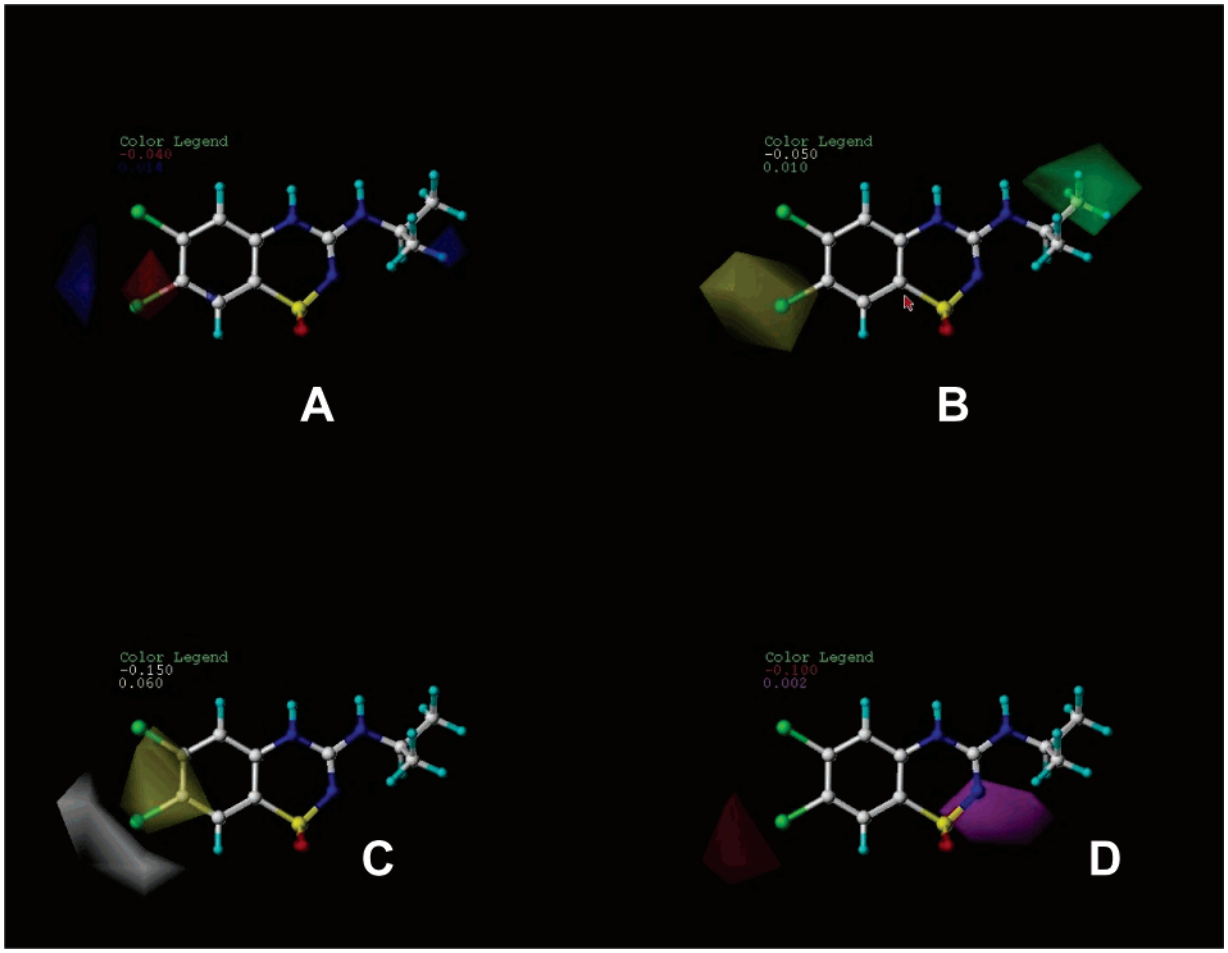

Figure 6. CoMSIA contour maps for the selectivity model: (A) electrostatic properties, the blue isocontours denote regions where negatively charged groups decrease the selectivity for the pancreatic tissue (contour level 0.014) and red areas indicate a deleterious effect of negatively charged groups for the inhibition of insulin release (contour level −0.040); (B) steric properties, sterically favorable areas to selectivity for the pancreatic tissue are shown in green (contour level 0.010), while the yellow isocontours depict sterically deleterious areas for the pancreatic tissue or favorable to the aortic tissue selectivity (contour level −0.050); (C) hydrophobic properties, yellow polyhedra (contour level 0.060) indicate regions where hydrophobic groups could enhance the selectivity for the pancreatic tissue and white areas (contour level −0.150) depict regions where hydrophilic groups could favor the selectivity for the aortic tissue; (D) H-bond acceptor properties, magenta isocontours (contour level 0.002) depict areas where H-bond acceptors on the molecule (or H-bond donors on the receptor site) could enhance the selectivity for the pancreatic tissue; the corresponding unfavorable areas are shown in red (contour level −0.100).

Concerning the electrostatic field properties (Figure 6A), it should be noticed that a small electronegative group (red) centered on the substituent in the 7-position could increase the activity but also the selectivity for the pancreatic tissue. A blue field near the 7-position seems to indicate a deleterious negatively charged zone for the inhibition of insulin release but a favorable zone for the vasorelaxant effect. Interpretation of the map at the 3-position appears too complex.

At the steric level, we can observe the presence of a unique zone (green) favorable to selectivity for the pancreatic tissue and located on one side of the chain in the 3-position (Figure 6B). This feature could confirm that only small and branched alkylamino side chains in the 3-position led to pancreatic selective drugs. By contrast, a large yellow zone near the substituent at the 7-position indicates that a bulky substituent in this position could decrease the selectivity for the pancreatic tissue and increase the selectivity for the aortic tissue. No critical information appears for the 6-position.

The analysis of the hydrophobic map (Figure 6C) seems to demonstrate the importance, for tissue selectivity, of the subtituent at the 7-position. Indeed, while a hydrophobic zone (yellow) centered on the substituent in the 7-position appears to be favorable for the inhibition of insulin release, the bulkiest hydrophobic groups were found to enter in a hydrophilic zone (white) and to enhance the selectivity for aortic tissue.

The map showing the influence of the hydrogen bond acceptors is less easily explainable (Figure 6D). The magenta zone near the 2-position, indicating that the presence of a hydrogen acceptor could lead to an increase of selectivity for the pancreatic tissue, does not appear to be directly linked to a particular group. A deleterious zone (red) for hydrogen acceptors was present near the 7-position. This feature is in accordance with the CoMSIA analysis executed on the two pharmacological models and could indicate that the presence of bulky hydrogen bond acceptor groups at the 7-position is concomitant with a decrease in selectivity.

New Pharmacophoric Models. The Pancreatic Pharmacophoric Model. Figure 7 illustrates the improved pharmacophoric model for activity on the pancreatic tissue taking also into account the results obtained from the CoMSIA analysis of the selectivity model.

Several relevant pieces of information about the structure−activity relationships (SARs) for activity on the pancreatic tissue have been deduced from the graphical 3D views obtained with the CoMSIA analysis. These data not only confirm the first pharmacophoric model (Figure 3) but also clearly improve the

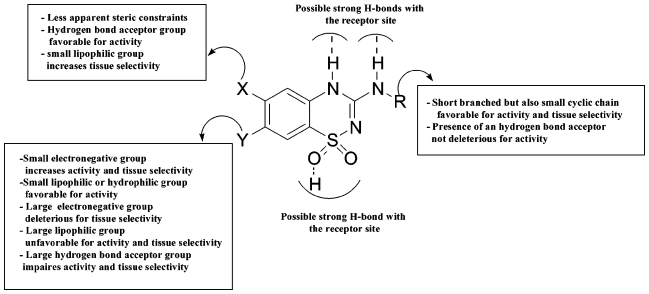

Figure 7. New improved pharmacophoric model for activity and selectivity on the pancreatic tissue.

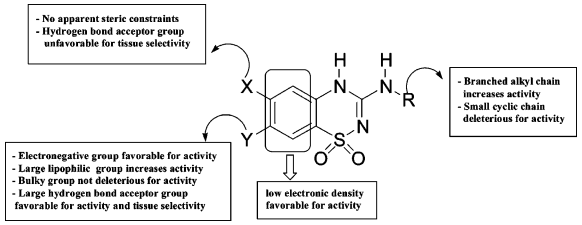

Figure 8. Pharmacophoric model for activity on the vascular smooth muscle tissue.

quality and the number of the SAR information concerning the arylthiadiazine 1,1-dioxide series. Indeed, the favorable and unfavorable lipophilic, steric, and electrostatic properties of the substituents at the 3- and at the 7-position are now better defined. Moreover, several pieces of information about substitution at the 6-position were added. Finally, thanks to the data collected from the CoMSIA analysis of the selectivity model, some relevant structural requirements for selectivity have been added to the initial pharmacophoric model.

As previously noted, the 3- and the 7-positions appear to be the key positions for activity but also for selectivity. In the 3-position, only short branched but also small cyclic chains such as cyclobutyl are shown to maintain or enhance activity and selectivity. Moreover, the presence of a hydrogen bond acceptor does not impair activity. Concerning the 7-position, the steric constraint is apparently the critical point, specifically for the pancreatic selectivity, while both small hydrophilic and hydrophobic groups enhance activity. No or less apparent steric constraints are demonstrated for the 6-position.

The Aortic Pharmacophoric Model. In the 3-alkylamino-benzo- and 3-alkylamino-pyridothiadiazine 1,1-dioxide series, no real SAR studies for the vascular smooth muscle tissue have been achieved up to now. Thus, the pharmacophoric model for activity on the vascular tissue presented in Figure 8 is the first one described for these series.

From the global analysis of this original model, it appears that activity on aortic K_{ATP} channels is less dependent on steric constraints than activity on pancreatic K_{ATP} channels. Moreover, lipophilicity at the 3-, 6-, and 7-positions is more critical in the aortic model, and a low electronic density on the aromatic ring is also favorable for potency.

This CoMSIA analysis also gives us an interesting predictive tool for the design of compounds activating the K_{ATP} channels of vascular smooth muscle.

Conclusions

Application of QSAR CoMFA or CoMSIA analysis to a huge series of potent PCOs belonging to the 3-alkylamino-4*H*-1,2,4-pyrido- and 3-alkylamino-4*H*-1,2,4-benzothiadiazine 1,1-dioxide series led to very coherent predictive models for activity on pancreatic and vascular tissues, as well as for tissue selectivity (pancreatic versus aortic). Moreover, examination of the different contour maps obtained by the CoMSIA analysis allowed the development of the first 3D pharmacophoric models for activity and selectivity on pancreatic and vascular tissues. The present work also highlighted the importance of the nature of the substituents at the 3- and 7-positions for both activity and tissue selectivity. Indeed, the steric bulk at these two positions appears to be critical for activity on the pancreatic tissue, while the presence of large electronegative or lipophilic groups at the 7-position enhance the activity on the vascular tissue. In contrast, the 6-position was not shown to be critical for activity or tissue selectivity. All this information, gathered in the new pharmacophoric models, can be viewed as very helpful for the rational design of potent and selective PCOs belonging to the arylthiadiazine series, and more specifically for the identification of a new pancreatic PCO of therapeutic value for the treatment or prevention of hyperinsulinemia, diabetes, and obesity.

Acknowledgment. This study was supported by grants from the National Fund for Scientific Research (F.N.R.S., Belgium) from which P. de Tullio is Research Associate and P. Lebrun Research Director. The authors gratefully acknowledge the technical assistance of P. Fraikin, F Leleux, A.-M. Vanbellinghen, and A. Van Praet.

Supporting Information Available: CoMSIA actual and predicted activities for the training and test set molecules. This material is available free of charge via the Internet at http://pubs.acs.org.

References

(1) Noma, A. ATP-regulated K^+ channels in cardiac muscle. *Nature* **1983**, *305*, 147−148.
(2) Cook, D. L.; Hales, C. N. Intracellular ATP directly blocks K^+ channels in pancreatic B-cells. *Nature* **1984**, *311*, 271−273.
(3) Bernardi, H.; Fosset, M.; Lazdunski, M. Purification and affinity labeling of brain [^{3}H] glibenclamide binding protein, a putative neuronal ATP-regulated K^+ channel. *Proc. Natl. Acad. Sci. U.S.A.* **1988**, *85*, 9816−9820.
(4) Standen, N. B.; Quayle, J. M.; Davies, N. W.; Brayden, J. E.; Huang, Y.; Nelson, M. T. Hyperpolarizing vasodilators activate ATP-sensitive K^+ channels in arterial smooth muscle. *Science* **1989**, *245*, 177−180.
(5) Allard, B.; Lazdunski, M. Pharmacological properties of ATP-sensitive K^+ channels in mammalian skeletal muscle cells. *Eur. J. Pharmacol.* **1993**, *236*, 419−426.
(6) Quayle, J. M.; Nelson, M. T.; Standen, N. B. ATP-sensitive and inwardly rectifying potassium channels in smooth muscle. *Physiol. Rev.* **1997**, *77*, 1165−1232.
(7) Bryan, J.; Aguilar-Bryan, L. The ABCs of ATP-sensitive potassium channels: More pieces of the puzzle. *Curr. Opin. Cell Biol.* **1997**, *9*, 553−559.
(8) Seino, S.; Miki, T. Physiological and pathophysiological roles of ATP-sensitive K^+ channels. *Prog. Biophys. Mol. Biol.* **2003**, *81*, 133−176.
(9) Babenko, A. P.; Aguilar-Bryan, J. A. A view of SUR/Kir6.X K_{ATP} channels. *Annu. Rev. Physiol.* **1998**, *60*, 667−687.
(10) D'hahan, N.; Jacquet, H.; Moreau, C.; Catty, P.; Vivaudou, M. A transmembrane domain of the sulfonylurea receptor mediates activation of ATP-sensitive K^+ channels by K^+ channel openers. *Mol. Pharmacol.* **1999**, *56*, 308−315.
(11) Seino, S. ATP-sensitive potassium channels: a model of heteromultimeric potassium channel/receptor assemblies. *Annu. Rev. Physiol.* **1999**, *61*, 337−362.
(12) Inagaki, N.; Gonio, T.; Clement, J. P. Reconstitution of I_{KATP}: An inward rectifier subunit plus a sulfonylurea receptor. *Science* **1995**, *270*, 1166−1170.
(13) Hambrock, A.; Löffler-Walz, C.; Kloor, D.; Delabar, U.; Horio, Y.; Kurachi, Y.; Quast, U. ATP-sensitive K^+ channel modulator binding to sulfonylurea receptors SUR2A and SUR2B: Opposite effects of MgADP. *Mol. Pharmacol.* **1999**, *55*, 832−840.
(14) Petersen, O. H.; Dunne, M. J. Regulation of K^+ channels plays a crucial role in the control of insulin secretion. *Pflüegers Arch.* **1989**, *414*, S115−S120.

(15) Lebrun, P. Flux cationiques dans les cellules B des îlots pancréatiques et investigations pharmacologiques. *Rev. Fr. Endocrinol. Clin.* **1993**, *34*, 241−254.
(16) Kolb, H. A. Potassium channels in excitable and non-excitable cells. *Rev. Physiol. Biochem. Pharmacol.* **1990**, *15*, 51−79.
(17) Brayden, J. E. Functional roles of K_{ATP} channels in vascular smooth muscles. *Clin. Exp. Pharmacol. Physiol.* **2002**, *29*, 312−316.
(18) Seino, S.; Miki, T. Physiological and pathophysiological roles of ATP-sensitive K^+ channels. *Prog. Biophys. Mol. Biol.* **2003**, *81*, 133−176.
(19) Coghlan, M. J.; Carroll, W. A.; Gopalakrishnan, M. Recent developments in the biology and medicinal chemistry of potassium channel modulators: Update from a decade of progress. *J. Med. Chem.* **2001**, *44*, 1627−1653.
(20) Lebrun, P.; Devreux, V.; Hermann, M.; Herchuelz, A. Similarities between the effects of pinacidil and diazoxide on ionic and secretory events in rat pancreatic islets. *J. Pharmacol. Exp. Ther.* **1989**, *250*, 1011−1018.
(21) Quast, U. Do the K^+ channel openers relax smooth muscle by opening K^+ channels? *Trends Pharmacol. Sci.* **1993**, *14*, 332−337.
(22) Mannhold, R. K_{ATP} channel openers: Structure−activity relationships and therapeutic potential. *Med. Res. Rev.* **2004**, *24*, 213−266.
(23) Björk, E.; Berne, C.; Kämpe, O.; Wibell, P.; Oskarsson, P.; Karlsson, F. A. Diazoxide treatment at onset preserves residual insulin secretion in adults with autoimmune diabetes. *Diabetes* **1996**, *45*, 1427−1430.
(24) Alemzadeh, R.; Langley, G.; Upchurch, L.; Smith, P.; Slonim, A. E. Beneficial effect of diazoxide in obese hyperinsulinemic adults. *J. Clin. Endocrinol. Metab.* **1998**, *83*, 1911−1915.
(25) Rasmussen, S. B.; Sorensen, T. S.; Hansen, J. B.; Mandrup-Poulsen, T.; Hornum, L.; Markholst, H. Functional rest through intensive treatment with insulin and potassium channel openers preserves residual beta-cells function and mass in acutely diabetic BB rats. *Horm. Metab. Res.* **2000**, *32*, 294−300.
(26) Ritzel, R. A.; Hansen, J. B.; Veldhuis, J. D.; Butler, P. C. Induction of beta-cell rest by a Kir6.2/SUR1-selective K(ATP)-channel opener preserves beta-cell insulin stores and insulin secretion in human islets cultured at high (11 mM) glucose. *J. Clin. Endocrinol. Metab.* **2004**, *89*, 795−805.
(27) Kumar, G. K.; Dastoor, F. C.; Robayo, J. R.; Razzaque, M. A. Side effects of diazoxide. *JAMA, J. Am. Med. Assoc.* **1976**, *235*, 275−276.
(28) de Tullio, P.; Pirotte, B.; Lebrun, P.; Fontaine, J.; Dupont, L.; Antoine, M.-H.; Ouedraogo, R.; Khelili, S.; Maggetto, C.; Masereel, B.; Diouf, O.; Podona, T.; Delarge, J. 3- and 4-Substituted 4*H*-pyrido[4,3-*e*]-1,2,4-thiadiazine 1,1-dioxides as potassium channel openers: Synthesis, pharmacological evaluation and structure−activity relationships. *J. Med. Chem.* **1996**, *39*, 937−948.
(29) de Tullio, P.; Ouedraogo, R.; Dupont, L.; Somers, F.; Boverie, S.; Dogné, J.-M.; Delarge, J.; Pirotte, B. Synthesis and structural studies of 3-alkylamino-pyrido[4,3-*e*]-1,2,4-thiadiazine 1,1-dioxides, a new class of heterocyclic compounds with therapeutic promises. *Tetrahedron* **1999**, *55*, 5419−5432.
(30) Pirotte, B.; Ouedraogo, R.; de Tullio, P.; Khelili, S.; Somers, F.; Boverie, S.; Dupont, L.; Fontaine, J.; Damas, J.; Lebrun, P. 3-Alkylamino-4*H*-pyrido[2,3-*e*]-1,2,4-thiadiazine 1,1-dioxides structurally related to diazoxide and pinacidil as potassium channel openers acting on vascular smooth muscle cells: Design, synthesis, and pharmacological evaluation. *J. Med. Chem.* **2000**, *43*, 1456−1466.
(31) Boverie, S.; Antoine, M.-H.; de Tullio,P.; Somers, F.; Becker, B.; Sebille, S.; Lebrun, P.; Pirotte, B. Effect on insulin release of compounds structurally related to the potassium-channel opener 7-chloro-3-isopropylamino-4*H*-1,2,4-benzothiadiazine 1,1-dioxide (BPDZ 73): Introduction of heteroatoms on the 3-alkylamino side chain of the benzothiadiazine 1,1-dioxide ring. *J. Pharm. Pharmacol.* **2001**, *53*, 973−980.
(32) Ouedraogo, R.; Becker, B.; Boverie, S.; Somers, F.; Antoine, M.-H.; Pirotte, B.; Lebrun, P.; de Tullio, P. 2-Alkyl-3-alkylamino-2*H*-benzo- and pyridothiadiazine 1,1-dioxides: From K^+_{ATP} channel openers to Ca^{2+} channel blockers? *Biol. Chem.* **2002**, *383*, 1759−1768.
(33) de Tullio, P.; Becker, B.; Boverie, S.; Dabrowski, M.; Wahl, P.; Antoine, M.-H.; Somers, F.; Sebille, S.; Ouedraogo, R.; Bondo Hansen, J.; Lebrun, P.; Pirotte, P. Toward tissue-selective pancreatic B-cells K_{ATP} channel openers belonging to 3-alkylamino-7-halo-4*H*-1,2,4-benzothiadiazine 1,1-dioxides. *J. Med. Chem.* **2003**, *46*, 3342−3353.
(34) Boverie, S.; Antoine, M.-H.; Somers, F.; Becker, B.; Sebille, S.; Ouedraogo, R.; Counerotte, S.; Pirotte, B.; Lebrun, P.; de Tullio, P. Effect on K_{ATP} channel activation properties and tissue selectivity of the nature of the substituent in the 7- and the 3-position of 4*H*-1,2,4-benzothiadiazine 1,1-dioxides. *J. Med. Chem.* **2005**, *48*, 3492−3503.
(35) de Tullio, P.; Boverie, S.; Becker, B.; Antoine, M.-H.; Nguyen, Q.-A.; Francotte, P.; Counerotte, S.; Sebille, S.; Pirotte, B.; Lebrun, P. 3-Alkylamino-4*H*-1,2,4-benzothiadiazine 1,1-dioxides as ATP-sensitive potassium channel openers: Effect of 6,7-disubstitution on potency and tissue selectivity. *J. Med. Chem.* **2005**, *48*, 4990−5000.
(36) Pirotte, B.; Antoine, M.-H.; de Tullio, P.; Hermann, M.; Herchuelz, A.; Delarge, J.; Lebrun, P. A pyridothiadiazine (BPDZ 44) as a new and potent activator of ATP-sensitive K^+ channels. *Biochem. Pharmacol.* **1994**, *47*, 1381−1386.
(37) Lebrun, P.; Arkhammar, P.; Antoine, M.-H.; Nguyen, Q.-A.; Bondo Hansen, J.; Pirotte, B. A potent diazoxide analogue activating ATP-sensitive K^+ channels and inhibiting insulin release. *Diabetologia* **2000**, *43*, 723−732.
(38) Cosgrove, K.; Antoine, M.-H.; Lee, A.; Barnes, P.; de Tullio, P.; Clayton, P.; McCloy, R.; De Lonlay, P.; Nihoul-Fékété, C.; Robert, J.; Saudubray, J.-M.; Rahier, J.; Lindley, K.; Hussain, K.; Aynsley-Green, A.; Pirotte, B.; Lebrun, P.; Dunne, M. BPDZ 154 activates adenosine 5′-triphosphate-sensitive potassium channels: In vitro studies using rodent insulin-secreting cells and islets isolated from patients with hyperinsulinism. *J. Clin. Endocrinol. Metab.* **2002**, *87*, 4860−4868.
(39) Dabrowski, M.; Ashcroft, F. M.; Ashfield, R.; Lebrun, P.; Pirotte, B.; Egebjerg, J.; Hansen J. B.; Wahl, P. The novel diazoxide analog 3-isopropylamino-7-methoxy-4*H*-1,2,4-benzothiadiazine 1,1-dioxide is a selective Kir6.2/SUR1 channel opener. *Diabetes* **2002**, *51*, 1896−1906.
(40) Nielsen, F. E.; Bodvarsdottir, T. B.; Worsaae, A.; MacKay, P.; Stidsen, C. E.; Boonen, H. C.; Pridal, L.; Arkhammar, P. O. G.; Whal, P.; Ynddal, L.; Junager, F.; Dragsted, N.; Tagmose, T. M.; Mogensen, J. P.; Koch, A.; Treppendahl, S. P.; Hansen, J. B. 6-Chloro-3-alkylamino-4*H*-thieno[3,2-*e*]-1,2,4-benzothiadiazine 1,1-dioxide derivatives potently and selectively activate ATP sensitive potassium channels of pancreatic beta-cells. *J. Med. Chem.* **2002**, *45*, 4171−4187.
(41) Pirotte, B.; de Tullio, P.; Antoine, M.-H.; Sebille, S.; Florence, X.; Lebrun, P. New insights into the development of ATP-sensitive potassium channel openers. *Expert Opin. Ther. Patents* **2005**, *15*, 497−504.
(42) *Sybyl 7.0*; Tripos Associates, Inc.: St. Louis, MO, 2004.
(43) Stewart, J. J. MOPAC, a Semiempirical Molecular Orbital Program. *J. Comput.-Aided Mol. Des.* **1990**, *4*, 1−105.
(44) Khelili, S.; de Tullio, P.; Lebrun, P.; Fillet, M.; Antoine, M.-H.; Ouedraogo, R.; Dupont, L.; Fontaine, J.; Felekidis, A.; Leclerc, G.; Delarge, J.; Pirotte, B. Preparation and pharmacological evaluation of the *R*- and *S*-enantiomers of 3-(2′-butylamino)-4*H*- and 3-(3′-methyl-2-butylamino)-4*H*-pyrido[4,3-*e*]-1,2,4-thiadiazine 1,1-dioxide, two tissue selective ATP-sensitive potassium channel openers. *Bioorg. Med. Chem.* **1999**, *7*, 1513−1520.
(45) Cramer, R. D., III; Bunce, J. D.; Patterson, D. E. Crossvalidation, bootstrapping, and partial least squares compared with multiple regression in conventional QSAR studies. *Quant. Struct.−Act. Relat.* **1988**, *7*, 18−25.

JM060534W